This is a repository copy of *Experimental Observation of Dual Magnetic States in Topological Insulators*.

White Rose Research Online URL for this paper:
https://eprints.whiterose.ac.uk/167242/

Version: Published Version

Article:

CONDENSED MATTER PHYSICS

Experimental observation of dual magnetic states in topological insulators

Wenqing Liu[1,2], Yongbing Xu[1,3]*, Liang He[1,4]*, Gerrit van der Laan[5], Rong Zhang[2], Kang Wang[4]*

The recently discovered topological phase offers new possibilities for spintronics and condensed matter. Even insulating material exhibits conductivity at the edges of certain systems, giving rise to an anomalous quantum Hall effect and other coherent spin transport phenomena, in which heat dissipation is minimized, with potential uses for next-generation energy-efficient electronics. While the metallic surface states of topological insulators (TIs) have been extensively studied, direct comparison of the surface and bulk magnetic properties of TIs has been little explored. We report unambiguous evidence for distinctly enhanced surface magnetism in a prototype magnetic TI, Cr-doped Bi_2Se_3. Using synchrotron-based x-ray techniques, we demonstrate a "three-step transition" model, with a temperature window of ~15 K, where the TI surface is magnetically ordered while the bulk is not. Understanding the dual magnetization process has strong implications for defining a physical model of magnetic TIs and lays the foundation for applications to information technology.

INTRODUCTION

Three-dimensional (3D) topological insulators (TIs) feature novel phases of quantum matter with sharp transitions in the electronic structure near their surfaces. Unlike the divergent electronic properties of surface and bulk regions of all solids owing to the inevitable termination of the periodic lattice structure when approaching the boundaries, TIs present a new class of nontrivial surface states arising from intrinsic strong spin-orbit coupling and characterized by Rashba spin texture (1–5). These low-dimensional surface states are immune to localization caused by disorders as long as the disorder potential is time-reversal invariant and therefore have strong implications for emerging technologies such as dissipationless transport and quantum computation (6, 7). Breaking the time-reversal invariance by introducing magnetic perturbation, on the other hand, reveals a complex phenomenology associated with a tunable excitation bandgap of the surface spectrum (8, 9), as illustrated in Fig. 1A. Such a magnetic TI system resembles that of a massive Dirac fermion, which represents an ideal laboratory to study the interplay between magnetism and topology (10–15).

While the presence of the metallic surface state has been well studied (1–14), experimental evidence on the magnetic properties of the TI surface is far from conclusive. It has been proposed that, in magnetic TIs, ferromagnetism can be developed not only through the van Vleck mechanism (10, 16), by which magnetic ions are directly coupled through the local valance electrons, but also the carrier-mediated Ruderman-Kittel-Kasuya-Yosida (RKKY) interaction when Fermi energy (E_F) is close to the Dirac point (17, 18). The surface versus bulk magnetization of a magnetic TI reflects a central question of topology: the role of dimensionality. In general, ordered phenomena, e.g., magnetic, superconducting order, and lattice stability etc., show fragility when the dimension of the system decreases ($T_c^{3D} > T_c^{2D}$) (here, T_c refers to the critical temperature of ordered phenomena in general). However, in the case of 3D TIs, the opposite can occur, such that $T_c^{surface} > T_c^{bulk}$, because of the unusual properties of the mediated helical electrons (19). Measurements show that the Dirac gap of a TI emerges independently of the bulk magnetic ordering (9). A number of recent reports on 3D magnetically-doped TIs including Mn-doped $Bi_2(TeSe)_3$ (20), Cr-doped $(BiSb)_2Te_3$ (21), Cr-doped $(Bi_xSb_{1−x})_2Te_3$ (16), and V-doped Sb_2Te_3 (22, 23) seem to be arriving at a consensus that surface magnetization is primarily predominated by the RKKY mechanism, while that of the bulk is steered by the van Vleck interaction. Nevertheless, the key issue of the dual magnetic states of 3D TIs, i.e., that the surface has a different magnetic moment and ordering temperature than that of the bulk, has yet to be established. Delicate techniques such as time-resolved angular-resolved photoemission spectroscopy, have been performed to distinguish bulk and surface electron-phonon coupling of the bare TI (24). With respect to magnetic TIs, β-nuclear magnetic resonance was used for depth profiling the electronic wave functions at topological surfaces (25).

It is possible to distinguish the surface moment of a magnetic TI from that of the bulk using the synchrotron-based x-ray absorption technique. This method is based on the modified surface band structure, i.e., surface-atom core-level shift (26–28), which is reflected in a different surface valance state of metallic elements and can be experimentally observed in their characteristic x-ray absorption spectroscopy (XAS) spectra. Tuning the absorption to the magnetic resonant edges, x-ray magnetic circular dichroism (XMCD) can be obtained for the surface and bulk dopants, respectively, revealing the magnetic ground state and temperature dependence in an unambiguous surface bulk–resolved manner. Here, we present a study of a prototype magnetic TI, i.e., Cr-doped Bi_2Se_3 in its ultrathin limit that is expected to give rise to the quantum anomalous Hall effect (10). Three kinds of samples were measured as illustrated in Fig. 1B. In the global-doped Bi_2Se_3 thin films, the Cr dopants are uniformly distributed throughout the sample, whereas in the modulation-doped Bi_2Se_3 thin films, the dopants are only introduced either into the topmost (referred as surf-doped) or the middle (referred as mid-doped) quintuple layer (QL), respectively. This was achieved by accurately controlling the dopant distribution profiles along the

[1]York-Nanjing Joint Center (YNJC) for Spintronics and Nanoengineering, School of Electronics Science and Engineering, Nanjing University, Nanjing 210093, China. [2]Department of Electronic Engineering, Royal Holloway University of London, Egham TW20 0EX, UK. [3]Department of Electronic Engineering, The University of York, York YO10 5DD, UK. [4]Department of Electrical and Computer Engineering, Department of Materials Science and Engineering, and Department of Physics, University of California, Los Angeles, Los Angeles, CA 90095, USA. [5]Magnetic Spectroscopy Group, Diamond Light Source, Didcot OX11 0DE, UK.
*Corresponding author. Email: yongbing.xu@york.ac.uk (Y.X.); heliang@nju.edu.cn (L.H.); wang@seas.ucla.edu (K.W.)
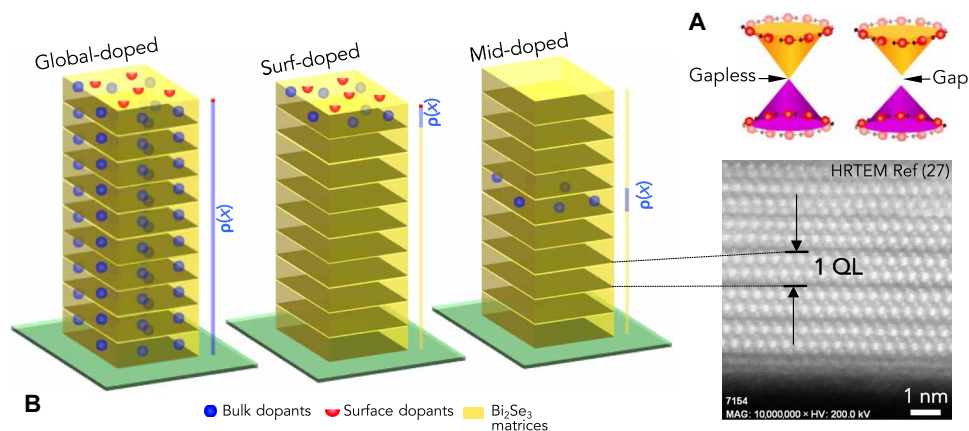
Fig. 1. Experimental configuration. (**A**) Conceptual illustration of the Dirac fermion states of the Bi_2Se_3 topological insulator. In the magnetically doped Bi_2Se_3 (right), a bandgap is present between the upper and lower Dirac cones. (**B**) Sample configuration of the global-, surf-, and mid-doped Bi_2Se_3. Each cuboid represents one Bi_2Se_3 quintuple layer (QL).
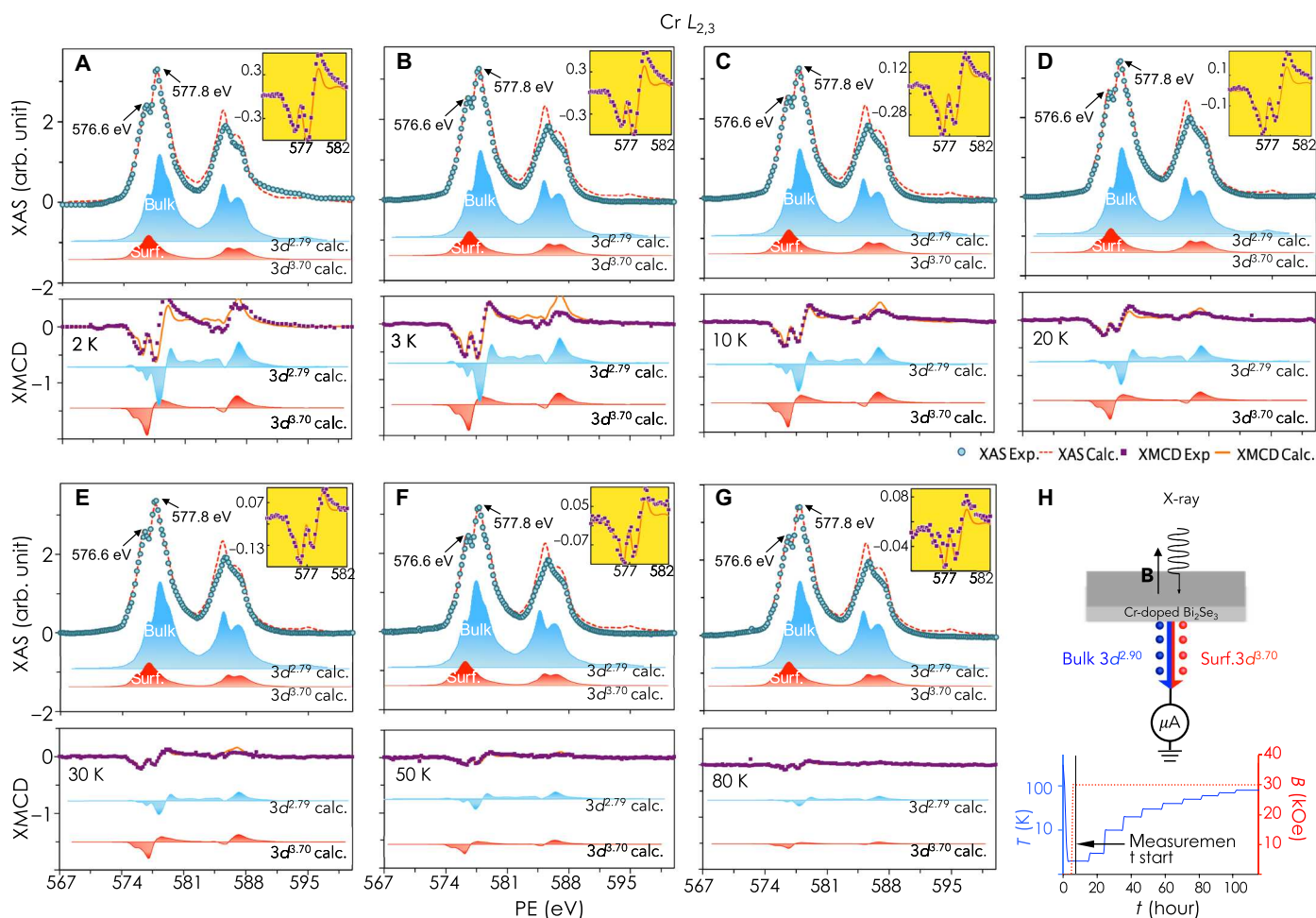

Fig. 2. The global-doped Bi_2Se_3. (**A** to **G**) Typical total XAS and XMCD and their deconvoluted spectra of the global-doped Bi_2Se_3 at 2 to 80 K, respectively. The (percentage) XMCD intensity at the Cr L_3 edge decreases with the increasing temperature within the measured range. The best fitting was obtained by a linear superposition of $d_{surf}^{3.70}$ and $d_{bulk}^{2.79}$, with ~1:3 for the total XAS and ~1:2 for the XMCD. (**H**) Schematic diagram of the experimental set up and the measurement processes. Circularly polarized x-rays were used in normal incidence with respect to the sample plane and parallel to the applied magnetic field. Samples were cooled down to 2 K without magnetic field, and data were collected in the warm-up cycle.

growth direction using the slow-deposition molecular beam epitaxy technique (see the Supplementary Materials).

RESULTS

We first address the dual magnetic states observed in the global-doped sample, i.e., 10-nm 3% Cr-doped Bi_2Se_3 epitaxial thin films. Figure 2 (A to G) present the measured total XAS and the XMCD spectra at the Cr $L_{2,3}$ edge of the global-doped Bi_2Se_3 thin film obtained in the total electron yield (TEY) mode (see the Supplementary Materials). The total XAS of Cr shows remarkable multiplet structures separated by 1.2 eV at both spin-orbit split core levels, suggesting a mixture of divalent and trivalent Cr. Atomic multiplet calculations were performed to simulate the electric-dipole transitions, i.e., $3d^n \rightarrow 2p^5 3d^{n+1}$, to deconvolute the hybridized spectra (see the Supplementary Materials) (29, 30). The best fit was obtained by a linear superposition of covalent Cr $d^{3.70}$ (divalent) and $d^{2.79}$ (trivalent) with ~1:3 for the total XAS, while this ratio is ~1:3 at 3 K and goes all the way up to ~1:1.5 at 80 K for the XMCD spectra. This suggests that, compared to the Cr $d^{3.70}$, the Cr $d^{2.79}$ loses magnetic ordering significantly faster with increasing temperature. The branching ratio (31), which quantifies the relative intensity of the L_3 edge in the total $L_{2,3}$ XAS intensity of the hybrid Cr $L_{2,3}$ XAS spectra,

is 0.63, standing in between 0.61 for $d^{2.79}$ and 0.68 for $d^{3.70}$ for the octahedral crystal-field symmetry.

Qualitatively, the contribution of the surface can be identified by comparing the spectra obtained in the bulk-sensitive total fluorescence yield (TFY) detection with that in the surface-sensitive TEY detection. While TEY at normal incidence probes only the top ~5 nm near the surface, TFY has a penetration depth of more than 100 nm (31, 32). In the global-doped Bi_2Se_3 thin film, the low-energy peak ($d^{3.70}$) is notably absent in the TFY spectrum, indicating that this peak originates from the top few atomic layers of the sample. First-principles density functional theory simulations confirm that this $d^{3.70}$ state is unlikely coming from any form of defects within Cr-doped Bi_2Se_3 (33). Note that the TEY intensity is attenuated by an exponentially decaying electron-escape probability. Therefore, in the total TEY-XAS spectra, the ratio of the Cr $d^{3.70}$ to Cr $d^{2.79}$ shows ~1:3 other than an unweighted sum of ~1:9 that one may tentatively assume.

We now have a picture that the two deconvoluted Cr $d^{3.70}$ and Cr $d^{2.79}$ spectra uniquely represent the surface and the bulk properties of the $Bi_{2-x}Cr_xSe_3$ and denote them as $d_{surf}^{3.70}$ and $d_{bulk}^{2.79}$, respectively, hereafter. Figure 3 (A and B, respectively) presents the total XAS and XMCD spectra of the modulation-doped Bi_2Se_3 thin films with an effective doping of 1.2% from 3 to 80 K. The deconvolution
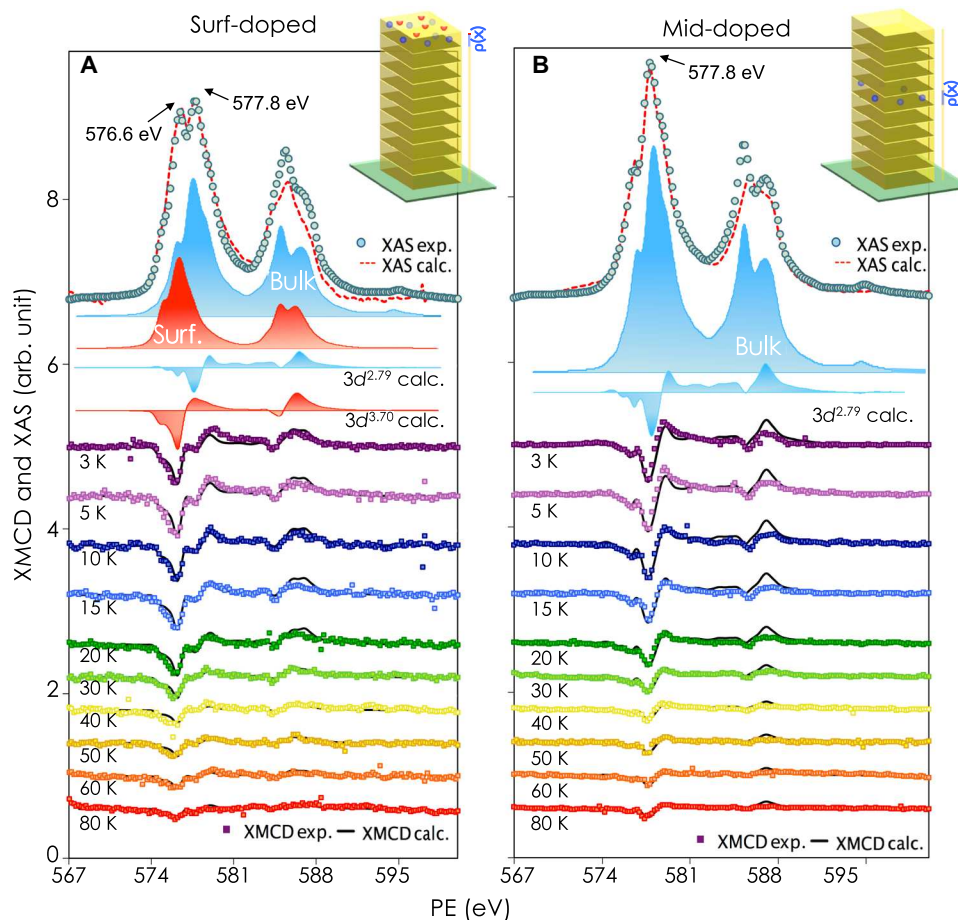

Fig. 3. The modulation-doped Bi_2Se_3. Typical total XAS and XMCD and their deconvoluted spectra of the (**A**) surf-doped and (**B**) mid-doped Bi_2Se_3 at 3 to 80 K, respectively. For the surf-doped Bi_2Se_3, the best fitting was obtained by a linear superposition of $d_{surf}^{3.70}$ and $d_{bulk}^{2.79}$, with ~4:5 for the total XAS and ~2:1 for the XMCD. No appreciable Cr $d_{surf}^{3.70}$ but only Cr $d_{bulk}^{2.79}$ was obtained from the mid-doped Bi_2Se_3.

of the total XAS gives the ratio of ~4:5 for the contribution of the Cr $d_{surf}{}^{3.70}$ and the Cr $d_{bulk}{}^{2.79}$ for the surf-doped sample, whereas no appreciable Cr $d_{surf}{}^{3.70}$ but only Cr $d_{bulk}{}^{2.79}$ was observed from the mid-doped sample. Note that even the surf-doped Bi_2Se_3 contains both Cr $d_{surf}{}^{3.70}$ and Cr $d_{bulk}{}^{2.79}$ with the later arising from the lower atomic sublayers of the first QL (see Fig. 1B). This is consistent with that observed for the global-doped sample.

Figure 4 presents the XMCD-derived spin (m_{spin}) and orbital (m_{orb}) magnetic moments versus temperature of the global- and the modulation-doped Bi_2Se_3, respectively, by applying sum rules to the separate XAS and XMCD spectra (see the Supplementary Materials). The XMCD-derived m_{spin} and m_{orb} of both the Cr $d_{surf}{}^{3.70}$ and Cr $d_{bulk}{}^{2.79}$ have opposite signs, corresponding to antiparallel alignment of the spin and orbital magnetization. This agrees with the Hund's rule for Cr, whose 3d shell is less than half full. For the global-doped Bi_2Se_3, we obtained a remarkable $m_{spin} = (3.44 \pm 0.30)$ μ_B/atom and a small negative $m_{orb} = (-0.06 \pm 0.03)$ μ_B/atom for the Cr $d_{surf}{}^{3.70}$, while those for the Cr $d_{bulk}{}^{2.79}$ are $m_{spin} = (1.65 \pm 0.30)$ μ_B/atom and $m_{orb} = (-0.09 \pm 0.03)$ μ_B/Cr at 3 K. For the modulation-doped Bi_2Se_3, the magnetization is slightly suppressed because of the reduced thickness of the doped region. We obtained $m_{spin} = (2.49 \pm 0.25)$ μ_B/atom and $m_{orb} = (-0.04 \pm 0.02)$ μ_B/atom for the Cr $d_{surf}{}^{3.70}$ of the surf-doped Bi_2Se_3. For the Cr $d_{bulk}{}^{2.79}$, the

magnetic moments extracted from the surf- and the mid-doped Bi_2Se_3 are identical within the experimental accuracy, namely, $m_{spin} = (1.30 \pm 0.10)$ μ_B/atom and $m_{orb} = (-0.14 \pm 0.02)$ μ_B/atom for the former and $m_{spin} = (1.34 \pm 0.10)$ μ_B/atom and $m_{orb} = (-0.15 \pm 0.02)$ μ_B/atom for the latter, respectively. While m_{orb} of the Cr $d_{bulk}{}^{2.79}$ for all the three samples is notably large, that of the Cr $d_{surf}{}^{3.70}$ is nearly quenched, which may be attributed to a slight distortion of the lattice symmetry of the surface.

DISCUSSION

In line with the electrical magnetotransport measurements (33), the XMCD-derived m_{spin} exhibits a Curie-like behavior, pointing to a ferromagnetic phase of the $Bi_{2-x}Cr_xSe_3$ thin film at low temperatures. The fact that the m_{spin} of the Cr $d_{surf}{}^{3.70}$ and the Cr $d_{bulk}{}^{2.79}$ of the global-doped Bi_2Se_3 show distinct temperature dependences points to the presence of dual magnetic states processing within one sample. As shown in Fig. 4, the Cr $d_{surf}{}^{3.70}$ exhibits more robust magnetization in both the magnitude of moment and the ordering temperature in comparison to that of the Cr $d_{bulk}{}^{2.79}$. Fitting the temperature-dependent magnetization within the mean-field approximation, i.e., $M(T) \propto (1 - T/T_c)^\gamma$, where γ represents the critical exponent, we obtained $T_c = (31.0 \pm 3.2)$ K and (31.3 ± 2.9) K for the Cr $d_{bulk}{}^{2.79}$ in the surf- and the mid-doped $Bi_{2-x}Cr_xSe_3$, respectively, and $T_c' = (46.4 \pm 2.5)$ K for the Cr $d_{surf}{}^{3.70}$ in the surf-doped $Bi_{2-x}Cr_xSe_3$. Table 1 summarizes the XMCD-derived m_s, T_c, and γ of the modulation-doped Bi_2Se_3 thin films.

Keeping in mind that the Cr $d_{bulk}{}^{2.79}$ and Cr $d_{surf}{}^{3.70}$ correspond to the two respective magnetization modes of the bulk and the surface, we conclude a "three-step-transition" model for the magnetic TIs against temperature. As illustrated in the upper row of Fig. 4: During phase I, both the surface and bulk are magnetically ordered below T_c; between T_c and T_c' (phase II), the surface retains magnetization while the bulk does not any longer; eventually, above T_c' (phase III), both the surface and the bulk lose their magnetic ordering. Note that, because electrical measurements are sensitive to the bulk, the transport-derived magnetically ordered temperatures (33) have a different physical meaning as those obtained using dichroic spectra and are rather close to the T_c of the Cr $d_{bulk}{}^{2.79}$. It is known that, in diluted magnetic semiconductors, ferromagnetic ordering is set via carrier-mediated exchange, which depends on the carrier concentration and, in turn, on the magnetic dopant concentration (34). The high density of free carriers required in these systems, however, is unsuitable for TIs (33). Theoretical predictions (17) indicate that the surface state–mediated spin-spin interaction is naturally ferromagnetic and even the bulk TI remains paramagnetic; experiments confirm that, in the magnetically doped Bi_2Se_3 systems, the Dirac gap in the surface spectrum can be present without bulk magnetic ordering (8, 9). A sharp transition of the magnetic susceptibility at the surface of TIs has been predicted
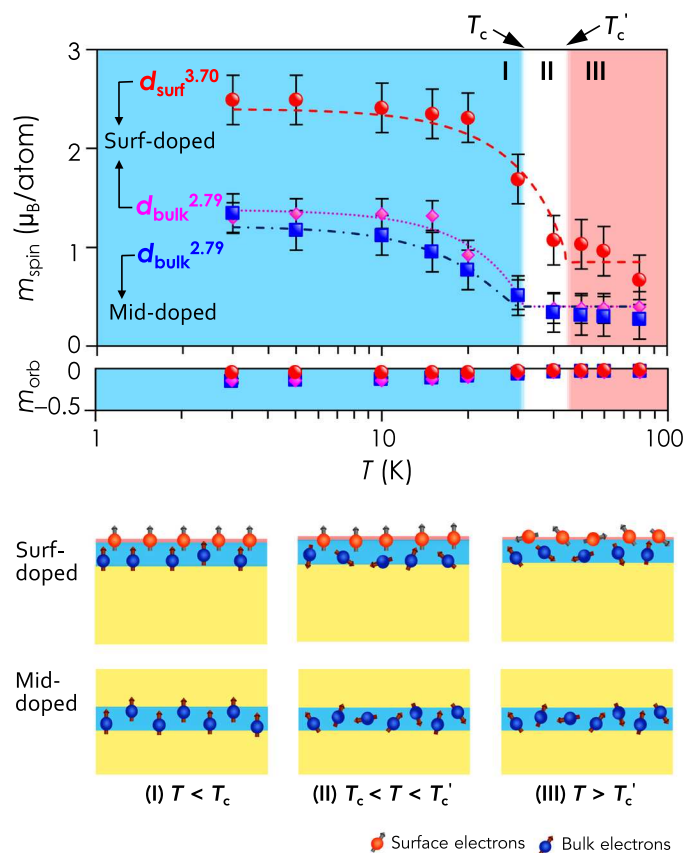

Fig. 4. M-T relationships. (Top) The XAS/XMCD-derived m_{spin} and m_{orb} of the $d_{surf}{}^{3.70}$ and $d_{bulk}{}^{2.79}$ versus temperature (T) at 3 to 80 K of the modulation-doped Bi_2Se_3 thin films. The dashed lines are the best fit within the mean-field approximation. **(Bottom)** Schematic illustration of the three-step transition: Both the surface and bulk are magnetically ordered below T_c (phase I); between T_c and T_c', the surface retains magnetization while the bulk does not anymore (phase II); eventually, beyond T_c', both the surface and bulk lose their magnetic orders (phase III).

Table 1. Summary of the XMCD-derived m_s, T_c, and γ of the modulation-doped Bi_2Se_3 thin films.

Sample	Cr dopants	m_s (μ_B/atom)	T_c (K)	γ
Surf-doped	$d_{surf}{}^{3.70}$	2.49 ± 0.25	46.4 ± 2.5	0.40 ± 0.14
	$d_{bulk}{}^{2.79}$	1.30 ± 0.10	31.0 ± 3.2	0.29 ± 0.17
Mid-doped	$d_{bulk}{}^{2.79}$	1.34 ± 0.10	31.3 ± 2.9	0.58 ± 0.10

(*35*) and demonstrated in experiment (*25*). Calculation (*19*) of the surface magnetic ordering of TIs has estimated values of 17.5 and 29 K, depending on the lattice model selected, for this temperature "window." This estimate compares well with our observation.

To conclude, we have defined and validated an experiential approach to determine the magnetic ground state in a "surface-specific" manner using synchrotron-based x-ray techniques. We have unambiguously observed an enhanced surface magnetic ordering of the $Bi_{2-x}Cr_xSe_3$ systems with a significantly large surface magnetic moment and high ordering temperature. We have demonstrated a three-step-transition model, in which a temperature window of ~15 K exists where the surface of the TI is magnetically ordered but the bulk is not. Future work to explore the tuning of this window and understand the dual magnetization process will have strong relevance to refining the physical model of magnetic TIs and lays the foundation for applications to emerging spintronic technologies.

MATERIALS AND METHODS

XAS and XMCD measurements at the Cr $L_{2,3}$ absorption edges of the $Bi_{2-x}Cr_xSe_3/Si(111)$ thin film were performed on beamline I10 at Diamond Light Source, UK. Circularly polarized x-rays with ~100% polarization were used in normal incidence with respect to the sample plane and parallel to the applied magnetic field, as illustrated in Fig. 2H. The XMCD was obtained by taking the difference of the XAS spectra, i.e., $\sigma^+ - \sigma^-$, by flipping the x-ray helicity at a fixed magnetic field of 30 kOe. The total XAS, on the other hand, was obtained by averaging over the two polarizations, i.e., $(\sigma^+ + \sigma^-)/2$. The intensity and the detailed line shape of the total XAS spectra reveal information of the Cr impurities in different valance states, while those of the XMCD spectra indicate the corresponding magnetic ground states. Atomic multiplet theory was used to calculate the electric-dipole transitions $3d^n \rightarrow 2p^5 3d^{n+1}$, where the spin-orbit and electrostatic interactions were treated on an equal footing (*36*). The wave functions of the initial- and final-state configurations were calculated in intermediate coupling using the Cowan's atomic Hartree-Fock (HF) code with relativistic corrections. The atomic electrostatic interactions include the $2p$-$3d$ and $3d$-$3d$ Coulomb and exchange interactions, which are reduced to 70% of their atomic HF value to account for the intra-atomic screening (*36*). Hybridization effects were included by mixing $3d^n$ with $3d^{n+1}L$ configurations, where L represents a hole on the neighboring atoms in states of appropriate symmetry. The Cr L_3 (L_2) line spectra were broadened by a Lorentzian with a half width at half maximum of $\Gamma = 0.3$ eV (0.4 eV) for intrinsic lifetime broadening and a Gaussian with an SD of $\sigma = 0.15$ eV for instrumental broadening.

SUPPLEMENTARY MATERIALS

Supplementary material for this article is available at http://advances.sciencemag.org/cgi/content/full/5/2/eaav2088/DC1
Section S1. Sample preparation
Section S2. XAS/XMCD measurement
Section S3. Multiplet calculations
Section S4. Sum-rules analysis
Fig. S1. Schematic diagram of the experimental setup for XAS and XMCD measurement.
Fig. S2. Deconvolution of the mixed Cr valences.
Fig. S3. The sum-rules analysis.
Table S1. Summary of the XMCD-derived m_{spin} for the global-, surf-, and mid-doped Cr-doped Bi_2Se_3, respectively, at 3 K.
References (*37–43*)

REFERENCES AND NOTES

1. C.-X. Liu, X.-L. Qi, X. Dai, Z. Fang, S.-C. Zhang, Quantum anomalous Hall effect in $Hg_{1-y}Mn_yTe$ quantum wells. *Phys. Rev. Lett.* **101**, 146802 (2008).
2. D. Hsieh, Y. Xia, D. Qian, L. Wray, J. H. Dil, F. Meier, J. Osterwalder, L. Patthey, J. G. Checkelsky, N. P. Ong, A. V. Fedorov, H. Lin, A. Bansil, D. Grauer, Y. S. Hor, R. J. Cava, M. Z. Hasan, A tunable topological insulator in the spin helical Dirac transport regime. *Nature* **460**, 1101–1105 (2009).
3. M. Z. Hasan, C. L. Kane, Colloquium: Topological insulators. *Rev. Mod. Phys.* **82**, 3045–3067 (2010).
4. A. Manchon, H. C. Koo, J. Nitta, S. M. Frolov, R. A. Duine, New perspectives for Rashba spin–orbit coupling. *Nat. Mater.* **14**, 871–882 (2015).
5. J. Wang, S.-C. Zhang, Topological states of condensed matter. *Nat. Mater.* **16**, 1062–1067 (2017).
6. D. N. Basov, R. D. Averitt, D. Hsieh, Towards properties on demand in quantum materials. *Nat. Mater.* **16**, 1077–1088 (2017).
7. D. Hsieh, Y. Xia, L. Wray, D. Qian, A. Pal, J. H. Dil, J. Osterwalder, F. Meier, G. Bihlmayer, C. L. Kane, Y. S. Hor, R. J. Cava, M. Z. Hasan, Observation of unconventional quantum spin textures in topological insulators. *Science* **323**, 919–922 (2009).
8. Y. L. Chen, J.-H. Chu, J. G. Analytis, Z. K. Liu, K. Igarashi, H.-H. Kuo, X. L. Qi, S. K. Mo, R. G. Moore, D. H. Lu, M. Hashimoto, T. Sasagawa, S. C. Zhang, I. R. Fisher, Z. Hussain, Z. X. Shen, Massive Dirac fermion on the surface of a magnetically doped topological insulator. *Science* **329**, 659–662 (2010).
9. L. A. Wray, S.-Y. Xu, Y. Xia, D. Hsieh, A. V. Fedorov, Y. S. Hor, R. J. Cava, A. Bansil, H. Lin, M. Z. Hasan, A topological insulator surface under strong Coulomb, magnetic and disorder perturbations. *Nat. Phys.* **7**, 32–37 (2011).
10. C.-Z. Chang, W. Zhao, D. Y. Kim, H. Zhang, B. A. Assaf, D. Heiman, S.-C. Zhang, C. Liu, M. H. W. Chan, J. S. Moodera, High-precision realization of robust quantum anomalous Hall state in a hard ferromagnetic topological insulator. *Nat. Mater.* **14**, 473–477 (2015).
11. R. Yu, W. Zhang, H.-J. Zhang, S.-C. Zhang, X. Dai, Z. Fang, Quantized anomalous Hall effect in magnetic topological insulators. *Science* **329**, 61–64 (2010).
12. C.-Z. Chang, J. Zhang, X. Feng, J. Shen, Z. Zhang, M. Guo, K. Li, Y. Ou, P. Wei, L.-L. Wang, Z.-Q. Ji, Y. Feng, S. Ji, X. Chen, J. Jia, X. Dai, Z. Fang, S.-C. Zhang, K. He, Y. Wang, L. Lu, X.-C. Ma, Q.-K. Xue, Experimental observation of the quantum anomalous Hall effect in a magnetic topological insulator. *Science* **340**, 167–170 (2013).
13. I. Garate, M. Franz, Inverse spin-galvanic effect in the interface between a topological insulator and a ferromagnet. *Phys. Rev. Lett.* **104**, 146802 (2010).
14. W. Liu, L. He, Y. Xu, K. Murata, M. C. Onbasli, M. Lang, N. J. Maltby, S. Li, X. Wang, C. A. Ross, P. Bencok, G. van der Laan, R. Zhang, K. L. Wang, Enhancing magnetic ordering in Cr-doped Bi_2Se_3 using high-T_C ferrimagnetic insulator. *Nano Lett.* **15**, 764–769 (2015).
15. W. Liu, Y. Xu, Magnetic two-dimensional systems. *Curr. Opin. Solid State Mater. Sci.* **20**, 388–395 (2016).
16. X. Kou, M. Lang, Y. Fan, Y. Jiang, T. Nie, J. Zhang, W. Jiang, Y. Wang, Y. Yao, L. He, K. L. Wang, Interplay between different magnetisms in Cr-doped topological insulators. *ACS Nano* **7**, 9205–9212 (2013).
17. Q. Liu, C.-X. Liu, C. Xu, X.-L. Qi, S.-C. Zhang, Magnetic impurities on the surface of a topological insulator. *Phys. Rev. Lett.* **102**, 156603 (2009).
18. J.-J. Zhu, D.-X. Yao, S.-C. Zhang, K. Chang, Electrically controllable surface magnetism on the surface of topological insulators. *Phys. Rev. Lett.* **106**, 097201 (2011).
19. G. Rosenberg, M. Franz, Surface magnetic ordering in topological insulators with bulk magnetic dopants. *Phys. Rev. B* **85**, 195119 (2012).
20. J. G. Checkelsky, J. Ye, Y. Onose, Y. Iwasa, Y. Tokura, Dirac-fermion-mediated ferromagnetism in a topological insulator. *Nat. Phys.* **8**, 729–733 (2012).
21. C.-Z. Chang, J. Zhang, M. Liu, Z. Zhang, X. Feng, K. Li, L.-L. Wang, X. Chen, X. Dai, Z. Fang, X.-L. Qi, S.-C. Zhang, Y. Wang, K. He, X.-C. Ma, Q.-K. Xue, Thin films of magnetically doped topological insulator with carrier-independent long-range ferromagnetic order. *Adv. Mater.* **25**, 1065–1070 (2013).
22. M. Li, C.-Z. Chang, L. Wu, J. Tao, W. Zhao, M. H. W. Chan, J. S. Moodera, J. Li, J. Zhu, Experimental verification of the Van Vleck nature of long-range ferromagnetic order in the Vanadium-doped three-dimensional topological insulator Sb_2Te_3. *Phys. Rev. Lett.* **114**, 146802 (2015).
23. P. Sessi, R. R. Biswas, T. Bathon, O. Storz, S. Wilfert, A. Barla, K. A. Kokh, O. E. Tereshchenko, K. Fauth, M. Bode, A. V. Balatsky, Dual nature of magnetic dopants and competing trends in topological insulators. *Nat. Commun.* **7**, 12027 (2016).
24. J. A. Sobota, S.-L. Yang, D. Leuenberger, A. F. Kemper, J. G. Analytis, I. R. Fisher, P. S. Kirchmann, T. P. Devereaux, Z.-X. Shen, Distinguishing bulk and surface electron-phonon coupling in the topological insulator Bi_2Se_3 using time-resolved photoemission spectroscopy. *Phys. Rev. Lett.* **113**, 157401 (2014).
25. D. Koumoulis, G. D. Morris, L. He, X. Kou, D. King, D. Wang, M. D. Hossain, K. L. Wang, G. A. Fiete, M. G. Kanatzidis, L.-S. Bouchard, Nanoscale β-nuclear magnetic resonance depth imaging of topological insulators. *Proc. Natl. Acad. Sci. U.S.A.* **112**, E3645–E3650 (2015).

26. P. H. Citrin, G. K. Wertheim, Y. Baer, Core-level binding energy and density of states from the surface atoms of gold. *Phys. Rev. Lett.* **41**, 1425–1428 (1978).

27. B. Johansson, Valence state at the surface of rare-earth metals. *Phys. Rev. B* **19**, 6615–6619 (1979).

28. P. H. Citrin, G. K. Wertheim, Photoemission from surface-atom core levels, surface densities of states, and metal-atom clusters: A unified picture. *Phys. Rev. B* **27**, 3176–3200 (1983).

29. A. I. Figueroa, G. van der Laan, L. J. Collins-McIntyre, S.-L. Zhang, A. A. Baker, S. E. Harrison, P. Schönherr, T. Cibin, T. Hesjedal, Magnetic Cr doping of Bi_2Se_3: Evidence for divalent Cr from x-ray spectroscopy. *Phys. Rev. B* **90**, 134402 (2014).

30. B. T. Thole, G. Van Der Laan, J. C. Fuggle, G. A. Sawatzky, R. C. Karnatak, J.-M. Esteva, *3d* x-ray-absorption lines and the $3d^9 4f^{n+1}$ multiplets of the lanthanides. *Phys. Rev. B.* **32**, 5107–5118 (1985).

31. G. van der Laan, A. I. Figueroa, X-ray magnetic circular dichroism—A versatile tool to study magnetism. *Coord. Chem. Rev.* **277–278**, 95–129 (2014).

32. W. Liu, Q. Zhou, Q. Chen, D. Niu, Y. Zhou, Y. Xu, R. Zhang, J. Wang, G. van der Laan, Probing the buried magnetic interfaces. *ACS Appl. Mater. Interf.* **8**, 5752–5757 (2016).

33. W. Liu, D. West, L. He, Y. Xu, J. Liu, K. Wang, Y. Wang, G. van der Laan, R. Zhang, S. Zhang, K. L. Wang, Atomic-scale magnetism of Cr-doped Bi_2Se_3 thin film topological insulators. *ACS Nano* **9**, 10237–10243 (2015).

34. T. Dietl, A ten-year perspective on dilute magnetic semiconductors and oxides. *Nat. Mater.* **9**, 965–974 (2010).

35. M. M. Vazifeh, M. Franz, Spin response of electrons on the surface of a topological insulator. *Phys. Rev. B* **86**, 045451 (2012).

36. G. van der Laan, B. T. Thole, Strong magnetic x-ray dichroism in 2p absorption spectra of 3d transition-metal ions. *Phys. Rev. B* **43**, 13401–13411 (1991).

37. L. He, X. Kou, K. L. Wang, Review of 3D topological insulator thin-film growth by molecular beam epitaxy and potential applications. *Phys. Status Solidi Rapid Res. Lett.* **7**, 50–63 (2013).

38. L. He, F. Xiu, Y. Wang, A. V. Fedorov, G. Huang, X. Kou, M. Lang, W. P. Beyermann, J. Zou, K. L. Wang, Epitaxial growth of Bi_2Se_3 topological insulator thin films on Si (111). *J. Appl. Phys.* **109**, 103702 (2011).

39. X. F. Kou, W. J. Jiang, M. R. Lang, F. X. Xiu, L. He, Y. Wang, Y. Wang, X. X. Yu, A. V. Fedorov, P. Zhang, K. L. Wang, Magnetically doped semiconducting topological insulators. *J. Appl. Phys.* **112**, 063912 (2012).

40. X. Kou, L. He, M. Lang, Y. Fan, K. Wong, Y. Jiang, T. Nie, W. Jiang, P. Upadhyaya, Z. Xing, Y. Wang, F. Xiu, R. N. Schwartz, K. L. Wang, Manipulating surface-related ferromagnetism in modulation-doped topological insulators. *Nano Lett.* **13**, 4587–4593 (2013).

41. I. Vobornik, G. Panaccione, J. Fujii, Z.-H. Zhu, F. Offi, B. R. Salles, F. Borgatti, P. Torelli, J. P. Rueff, D. Ceolin, A. Artioli, M. Unnikrishnan, G. Levy, M. Marangolo, M. Eddrief, D. Krizmancic, H. Ji, A. Damascelli, G. van der Laan, R. G. Egdell, R. J. Cava, Observation of distinct bulk and surface chemical environments in a topological insulator under magnetic doping. *J. Phys. Chem. C* **118**, 12333–12339 (2014).

42. B. T. Thole, P. Carra, F. Sette, G. van der Laan, X-ray circular dichroism as a probe of orbital magnetization. *Phys. Rev. Lett.* **68**, 1943–1946 (1992).

43. P. Carra, B. T. Thole, M. Altarelli, X. Wang, X-ray circular dichroism and local magnetic fields. *Phys. Rev. Lett.* **70**, 694–697 (1993).

Citation: W. Liu, Y. Xu, L. He, G. van der Laan, R. Zhang, K. Wang, Experimental observation of dual magnetic states in topological insulators. *Sci. Adv.* **5**, eaav2088 (2019).

Science Advances

Experimental observation of dual magnetic states in topological insulators

Wenqing Liu, Yongbing Xu, Liang He, Gerrit van der Laan, Rong Zhang and Kang Wang

ARTICLE TOOLS	http://advances.sciencemag.org/content/5/2/eaav2088
SUPPLEMENTARY MATERIALS	http://advances.sciencemag.org/content/suppl/2019/02/04/5.2.eaav2088.DC1
REFERENCES	This article cites 43 articles, 5 of which you can access for free http://advances.sciencemag.org/content/5/2/eaav2088#BIBL
PERMISSIONS	http://www.sciencemag.org/help/reprints-and-permissions

Use of this article is subject to the Terms of Service